Nanostructured BaTi1-xSnxO3 ferroelectric materials for electrocaloric applications and energy performance

M. Benyoussef, T. Mura, S. Saitzek, F. Azrour, Jean-François Blach, A. Lahmar, Y. Gagou, M. El Marssi, Adlane Sayede, M. Jouiad

Nanostructured $BaTi_{1-x}Sn_xO_3$ ferroelectric materials for electrocaloric applications and energy performance

M. Benyoussef[a], T. Mura[b], S. Saitzek[b,*], F. Azrour[a], J.-F. Blach[b], A. Lahmar[a], Y. Gagou[a,*], M. El Marssi[a], A. Sayede[b], M. Jouiad[a,*]

[a]Laboratory of Physics of Condensed Matter, University of Picardie Jules Verne, Scientific Pole, 33 rue Saint-Leu, 80039 Amiens Cedex 1, France
[b]University of Artois, CNRS, Centrale Lille, Univ. Lille, UMR 8181, Unité de Catalyse et Chimie du Solide (UCCS), F-62300 Lens, France

Abstract

Nanostructured $BaTi_{1-x}Sn_xO_3$ (x = 0, 0.05 & 0.075) were successfully synthesized using the modified Pechini processing method. The phase purity and symmetry were examined by X-ray diffraction and Raman spectroscopy. Tetragonal symmetry was obtained for $BaTiO_3$ (BT) while orthorhombic symmetry for Sn doped BT. BT exhibits an up-shift of the Curie temperature towards high temperatures (T_C=139°C). In contrast, a down-shift was recorded for Sn doped BT. Then, indirect electrocaloric (EC) adiabatic temperature change ΔT and the energy storage performances were determined based on ferroelectric hysteresis loops. Interestingly, large EC responsivity of $\Delta T/\Delta E = 0.81\times10^{-6}$ K.m/V was obtained for the BT accompanied with a moderate stored energy of 23 mJ/cm^3 but with a high energy efficiency of 67%. The incorporation of Sn in BT was found to broaden the EC responsivity and to improve the energy efficiency up to 90%, recorded for the 5% Sn doped BT.

1. Introduction

Lead-based ferroelectric perovskites, such as $PbZr_{1-x}Ti_xO_3$ system, have attracted great interest owing to their interesting piezoelectric and ferroelectric properties, which makes them good candidates for technological and industrial applications [1–3]. However, due to the latest European directives on environmental and heath preservation, the use of lead in electrical and electronic components has been restricted [4]. Consequently, attention has been paid to the development of lead-free materials possessing performances that could compete with lead-based systems [5–7]. Owing to its remarkable dielectric, ferroelectric and piezoelectric properties combined with an excellent chemical and mechanical stability at room temperature [8], barium titanate $BaTiO_3$ (BT) material is considered a good alternative to lead-based systems for large-scale industrial applications [9–11]. Note that neat BT system presents three main phase transitions. A first paraelectric (cubic, *Pm3m*) to ferroelectric (tetragonal, *P4mm*) phase transition occurring at the Curie temperature, $T_C \sim 403$ K prone to grain size dependence [12]. A second phase transition towards an orthorhombic (*Amm2*) symmetry at 278 K, and a third one at 185 K towards a rhombohedral (*R3m*) symmetry [13]. The highest dielectric permittivity obtained near T_C is very interesting for practical applications such as energy conversion. Indeed, a giant EC effect was found near the sharp phase transition of BT system, demonstrating the high potential of BT-based materials for the development of functional cooling devices [14–16]. However, the sharp phase transition typical of the BT system presents some inherent limitations such as a very weak temperature stability preventing the increase of its dielectric and EC performances, and its high ferroelectric (FE) to paraelectric (PE) transition temperature that needs to be lowered to near ambient to respond to the actual capacitor's needs [17].

To improve the electrocaloric response of the BT, several works were oriented towards grain size engineering, doping, mechanical loading, and the coexistence of positive and negative electrocaloric effects. Indeed, Shan *et al.* recently demonstrated mechanical control of the EC response in BT-based epitaxial thin films [18]. These authors have also demonstrated a strategy to induce the coexistence of both positive and negative EC responses via electric-field-induced FE-FE phase transition in BT-based systems [19]. In addition, the impact of elements doping on EC was also considered on BT system, such as Ca^{2+}, Sr^{2+}, or Ce^{3+} incorporated in the Ba-site, and Mn^{3+}, Zr^{4+}, Sn^{4+}, Hf^{4+}, or Ce^{4+} incorporated in the Ti-site [20–25]. Particularly Sn^{4+} doping on the Ba-site in bulk systems was reported to improve the dielectric, FE, and EC performances

compared to the neat BT [23,26–28]. Moreover, grain size engineering was also reported to have a considerable impact on the EC performances of BT system [29–31].

In this work, we report on the elaboration and characterization of nanostructured $BaTi_{1-x}Sn_xO_3$ ceramics and their electrocaloric and energy storage performances. A special attention will be given to the effect of grain size and Sn doping on their structural and physical properties.

2. Experimental methods

Nanocrystalline $BaTi_{1-x}Sn_xO_3$ (BTxSn) powders (x = 0 – 7.5%) were prepared using the modified Pechini method [32]. The raw materials are titanium (IV) n-butoxide ($Ti(C_4H_9O)_4$ Strem Chemicals 98%), acetic acid (CH_3COOH, Sigma Aldrich, 99,7%), ethyl alcohol (C_2H_5OH, sigma Aldrich, >99%), barium acetate ($Ba(C_2H_3O_2)_2$, Strem chemicals 99%) and tin (IV) chloride pentahydrate ($SnCl_4,5H_2O$, Strem Chemicals, 98%). A first solution (A) is prepared by mixing in the following order the n-butoxide titanium, acetic acid and absolute ethanol in molar ratios 1:3:7 respectively. The mixing is then stirred until a clear solution is obtained. Titanium (IV) n-butoxide must not be placed in the presence of water in order to avoid its hydrolysis and the formation of insoluble clusters. A second solution (B) is prepared containing a stoichiometric mixture of tin and barium precursors to which acetic acid and ethanol are added with molar ratios of 1 (Ba/Sn):6:7, respectively. After complete dissolution, the two solutions A and B are vigorously stirred then placed in an oven at 90°C for 45 min to obtain a translucent to slightly cloudy gel. The gel is then calcined in air at 800°C for 6 hours (with heating/cooling ramps rate set at 5°C/min) to obtain nanosized $BaTi_{1-x}Sn_xO_3$ powders. Thermal analysis has been performed using a combined thermogravimetric analysis and differential scanning calorimetry TGA/DSC 3+ STARe System (Mettler Toledo). The scan rate is set to 5 °C/min under an air flow of 40 mL/min. X-Ray diffraction (XRD) patterns were collected using a Rigaku ULTIMA IV diffractometer equipped with Cu anticathode, Soller slits to limit the divergence of X-ray beam and a nickel foil filter attenuates the Cu K_β line. The registered angular range is 20°-80° at 0.1°/min scan resolution using the Bragg-Brentano configuration. Raman spectrometry was performed on Renishaw in Via system using green laser excitation (532 nm) at the power of 1 mW. The dielectric measurements were performed using a Solartron Impedance analyzer SI-12060. Ferroelectric hysteresis loops were collected at different temperatures using a ferroelectric test system (TF Analyzer 2000, aix-ACCT). Powder imaging were carried out using

environmental scanning electron microscopy ESEM Quanta 450 and the ceramic cross section was prepared by liquid nitrogen cleavage technique.

3. Results and discussions

3.1. Thermal analysis

Thermal stability of $BaTi_{1-x}Sn_xO_3$ (x = 0, 5%) oxides and their phase transitions examined by TGA/DSC is depicted in the fig. 1.

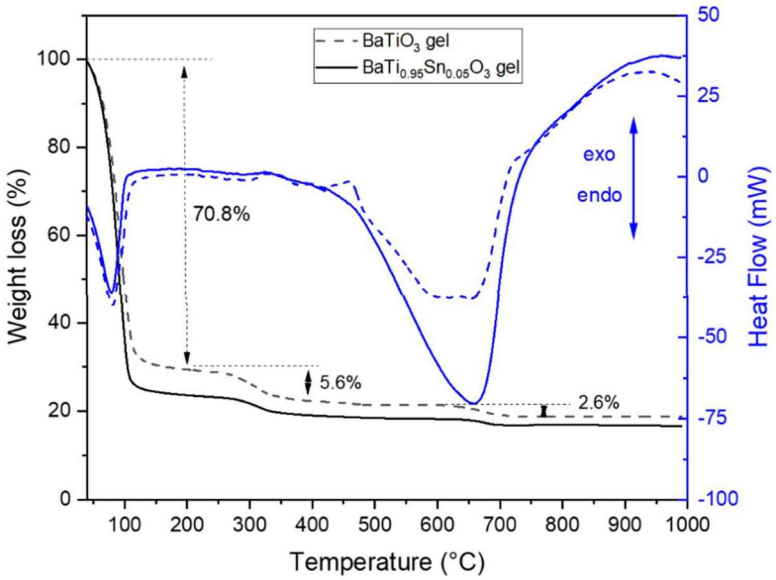

Fig. 1. $BaTiO_3$ and $BaTi_{0.95}Sn_{0.05}O_3$ gels thermal stability and phase transitions recorded in air during TGA/DSC experiment.

As can be seen in fig. 1, the BT weight loss shows three successive transitions: 1) 70.8% weight loss, located at relatively low temperatures (60-110°C), it is attributed to the evaporation of solvents such as water and ethanol present in the wet gel. This evaporation is confirmed by the endothermic heat flow characterized by the peak observed on the DSC signal; 2) 5.6% weight loss, located between 270 to 400°C, which is associated with the exothermic heat flow. This loss is attributed to in one hand, to the decomposition of titanium acetate into TiO_2 and acetic anhydride and to the decomposition of barium acetate into $BaCO_3$, in the other hand [33]; 3) 2.6 % weight loss, located at 610-650°C, which is attributed to the formation of $BaTiO_3$ and the release of CO_2 as byproduct through the reaction between $BaCO_3$ and TiO_2 [33]. Similarly, the $BaTi_{0.95}Sn_{0.05}O_3$ gel weight loss exhibits the same observed thermal decomposition as the BT gel without additional peak that could raise from the decomposition of tin salt. Indeed, the thermal

decomposition of tin (IV) chloride prepared in ethanol medium shows the formation of SnO_2 at a low temperature (< 300°C) [34].

3.2. Structural analysis

The morphology and the grain size of the as-processed BT and Sn doped BTxSn powders were observed in ESEM and given in fig. 2a-c.

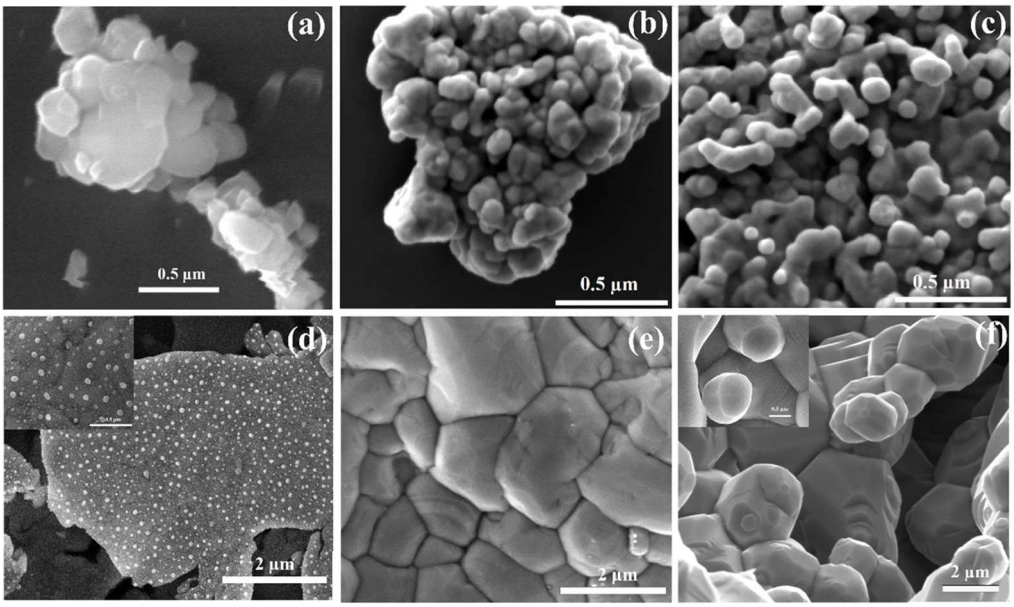

Fig. 2. SEM images of (a) $BaTiO_3$, (b) $BaTi_{0.95}Sn_{0.05}O_3$, and (c) $BaTi_{0.925}Sn_{0.075}O_3$ powders, and (d) $BaTiO_3$, (e) $BaTi_{0.95}Sn_{0.05}O_3$, and (f) $BaTi_{0.925}Sn_{0.075}O_3$ ceramics.

The examination of the as-processed powders (Fig. 2a-c) shows that the nanograins have a relatively spherical shape with 45 nm, 39 nm and 31 nm in diameter for BT, BT5%Sn doped, and BT7.5%Sn doped, respectively. After, casting and sintering, the grain size for the neat BT ceramic is about ~ 70 nm (e.g., fig. 2d) compared to doped compounds (e.g., fig. 2e, f), exhibiting larger grain sizes (1 – 4 µm).

X-ray diffraction patterns were recorded at room temperature for the three compounds as depicted in fig. 3.

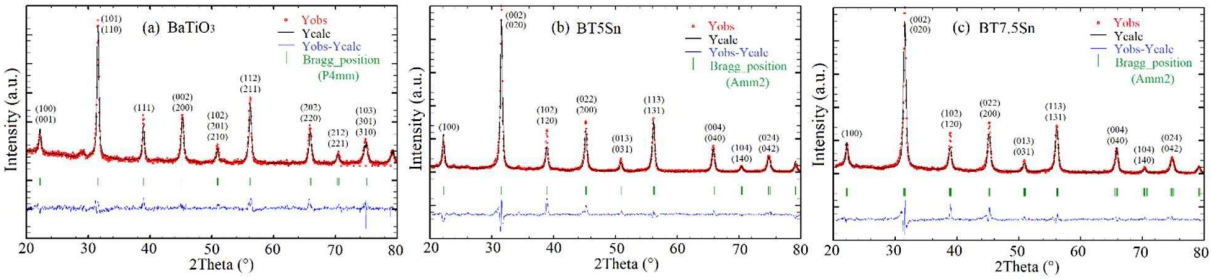

Fig. 3. XRD patterns of the BTxSn calcined in air at 800°C for 6 hours: a) x=0, b) x=5%, c) x=7.5%.

Structural investigations based on Rietveld calculations using Fullprof software [35] confirmed a tetragonal symmetry for BT nanostructured ceramic and an orthorhombic symmetry phase for both BT5%Sn and BT7.5%Sn. Our calculation approach considers as starting point, the tetragonal phase in *P*4*mm* (No 99) space group in pattern matching mode. As such, the calculation yielded to a rapid convergence for BT which allows coherent peak identification of the BT X-ray pattern [36]. In contrast, using the same approach for the Sn-doped BT compounds, it did not lead to conclusive results. Hence, different symmetry consideration were tested in accordance to bulk BTxSn phase diagram reported elsewhere [23,26] where BT doped with 5%Sn and 10%Sn-contents induced tetragonal-to-orthorhombic phase transition. Structural refinement was then conducted in the orthorhombic symmetry with *Amm*2 (No 39) as space group that led to satisfactorily results. Visual graphical criteria such as the plots of observed and calculated intensities and their difference instabilities due to the statistics of the recorded X-ray patterns but the reliability factors are conclusive. The plot on the bottom of fig. 3a-c, shows residual intensities due to line profiles, bad scaling parameters and bi-phased structure. Therefore, other assumption using phases mixture were considered but it was clear that the orthorhombic symmetry presents the major contribution.

Moreover, for the six-fold coordination, the Sn^{4+} ionic radius is greater than Ti^{4+}, hence the Sn substitution led to an increase in the lattice parameters according to Vegard's law (Table 1) [37]. Moreover, the well-known Scherrer formula was used to determine their crystallites size from the XRD data (Table 1) [38]. The obtained crystallite size was controlled by the processing temperature. Indeed, the sol-gel synthesis route makes it possible to obtain nanometric crystallites size. These crystallites may coalesce during the calcination carried out at high temperature. Here, we have chosen the lowest temperature 800°C, below which the precursors could not be entirely reacted to lead to the desired phase, favoring the obtained nanometric size. Note that the EC response was found to be directly related to the crystallites size, namely Patel *et al.* [39] have

described the influence of the grains size on the EC properties of $BaTiO_3$ and M. Kumar *et al.* [40] have reported an improved EC performance in doped $BaTiO_3$ possessing reduced grain size.

Table 1: Space group, lattice parameters, average crystallite size, and Rietveld refinement parameters of BTxSn.

%Sn	Space group	a (Å)	b (Å)	c (Å)	V (Å^3)	D (nm)	R_F	R_B
0	*P*4*mm*	3.99	3.99	4.01	64.18	43	5.55	7.45
5	*Amm*2	4.01	5.67	5.67	129.10	38	5.03	7.85
7.5	*Amm*2	4	5.66	5.70	129.25	33	8.3	5.8

By deconvolving the instrumental part across the Full Width at Half Maximum (FWHM), a slight decrease in crystallite size when x increases, is obtained. This trend agrees with the SEM observations. Atomic positions, isotropic thermal agitation parameters and occupancy of BTxSn ceramics are depicted in Table 2.

Table 2: Refined lattice parameters of BT (tetragonal *P*4*mm*), BT5%Sn (orthorhombic *Amm*2), and BT7.5%Sn (orthorhombic *Amm*2).

$BaTiO_3$						
Atom	Site	x	y	z	B(Å)	Occupancy
Ba	1a	0	0	0.10552	-0.099	1
Ti	1b	0.5	0.5	0.54338	-3.741	1
O_1	1b	0.5	0.5	0.04157	-2.384	1
O_2	2c	0.5	0	0.69073	-3.398	2
BT5Sn						
Ba	2a	0	0	-0.02445	-3.092	1
Ti/Sn	2b	0.5	0	-0.48254	3.795	0.95/0.05
O_1	2a	0	0	0.31689	2.510	1
O_2	4e	0	0.36845	0.21026	-3.364	2
BT7.5Sn						
Ba	2a	0	0	-0.02898	2.189	1
Ti/Sn	2b	0.5	0	0.46696	1.519	0.925/0.075
O_1	2b	0.5	0	0.27605	3.194	1
O_2	4d	0.5	0.26238	0.23701	-2.827	2

The obtained values show an average increase of lattice parameters due to the substitution of Ti (smaller ionic radius) by Sn larger ionic radius at the perovskite B-site. Furthermore, the thermal agitation parameters are abnormal. This is in favor to an additional symmetry contribution.

3.3. Raman spectroscopy

The room-temperature Raman spectra of the BTxSn (x = 0, 5%, 7.5%) ceramics synthesized using the sol-gel route are shown in fig. 4. Note that the spectra are Bose-Einstein corrected. Regarding the pure $BaTiO_3$ ceramic, Raman spectrum shows a highly damped soft mode, an interference dip at around 180 cm^{-1}, a broad band at ~270 cm^{-1} assigned to the A_1 (TO) mode, a sharp mode at ~307 cm^{-1} attributed to the B_1 + E (TO, LO) modes (‘‘silent’’ mode), an intense band at ~518 cm^{-1} attributed to the A_1 (TO) mode, and a high frequency mode at ~720 cm^{-1} assigned to the A_1 (LO) + E (LO) phonon modes (where the notation TO and LO denotes the transverse and longitudinal optical modes, respectively). Noting that the high wavenumber mode is reported to be related to the existence of oxygen vacancies [41,42]. It should also be mentioned that the presence of the interference dip and the sharp ‘‘silent’’ mode, are only observed in long-range FE phase [43]. The observed Raman modes are in good agreement with previous works reporting on the tetragonal (*P4mm*) structure of BT with a corresponding point group of symmetry C_{4v}^1[44–48]. Interestingly, the introduction of Sn element in $BaTiO_3$ matrix resulted in several changes on the Raman spectra. First, an underdamped soft mode can be observed for the Sn doped samples (obvious in the case of BT5%Sn) compared to the highly damped one of BT system. In addition, the A_1 (TO) ~270 cm^{-1} mode is observed to soften to ~250 cm^{-1} for the doped BTxSn compositions. The presence of the underdamped soft mode in addition to the frequency downshift of the A_1 (TO) mode are the signature of the orthorhombic (*Amm2*) symmetry [49], in good agreement with our structural findings. Moreover, a new interference dip is observed on the doped ceramics at ~130 cm^{-1}, which is probably due to the response of two different local octahedral environments owing to the involvement of cations with different ionic radii (Ti^{4+} and Sn^{4+}) in BTxSn system [12]. Besides, the presence of the ‘‘silent’’ mode in the doped samples indicates that the Sn-doping content preserves the long-range order of the FE BT system, especially in the case of the BT5%Sn system [50]. Moreover, we can observe an obvious broadening of all Raman modes as the doping content increases, resulting from the disorder induced by Sn introduction. Regarding the BT7.5%Sn sample, an evident broadening of the A_1 (TO) mode, in addition to the intensity decline of the ‘‘silent’’ mode and the reduction of the interference dip (180 cm^{-1}) express a reduction of the long-range FE ordering, as observed in $BaTi_{1-x}Zr_xO_3$ system [51].

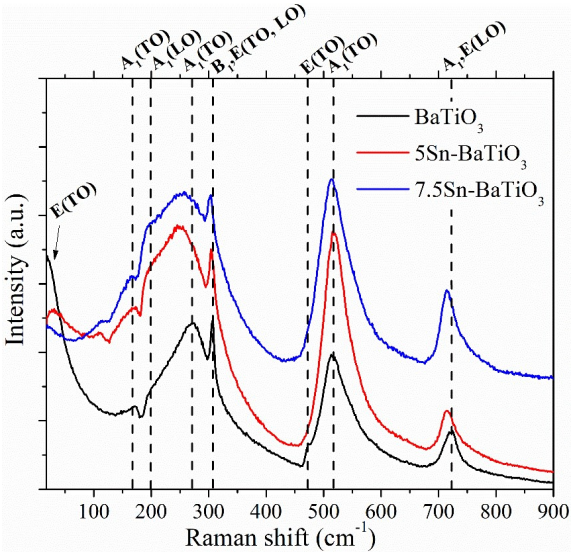

Fig. 4. Raman spectra of Sn^{4+} doped $BaTiO_3$ system. The modes assignments are shown in the tetragonal phase of bulk BT.

3.4. Dielectric properties

To determine the phase transition temperatures, dielectric properties measurements were carried on the samples. Fig. 5a-c presents the frequency and temperature dependence of the dielectric constant (ε_r) for the neat and Sn doped BT nanostructured systems.

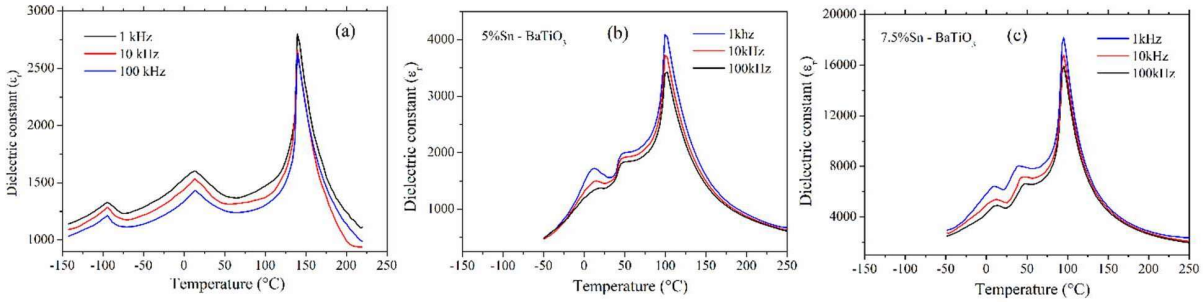

Fig. 5: Temperature and frequency dependence of the dielectric constant: a) $BaTiO_3$, b) $BaTi_{0.95}Sn_{0.05}O_3$, and c) $BaTi_{0.925}Sn_{0.075}O_3$.

One can observe in Fig. 5a, the presence of the three known phase transition temperatures ($T_{R\text{-}O}$, $T_{O\text{-}T}$, and $T_{T\text{-}C}$) in neat nanostructured BT as reported elsewhere [52]. However, here a slight shift toward high temperatures for $T_{T\text{-}C}$ is also observed. This could be attributed to the presence of polar nanoregions (PNRs) in nanostructured BT [53]. This induces the phase transformation towards the global symmetry at relatively higher temperature (~139°C) compared to bulk BT possessing larger FE domains. Besides, ε_r was found to be smaller to reported values for bulk BT system as reported elsewhere [54]. These authors showed significant decrease in the dielectric

permittivity values from $\varepsilon_r \sim 8000$ to $\varepsilon_r \sim 1000$, as grain size decreases from 500 nm to 50 nm, respectively [54]. Furthermore, the phase transition temperatures T_{R-O} and T_{O-T} remain very close to observed ones in bulk BT. This means that the dynamic of phase transformations mainly concerns FE-to-PE transition.

As can be seen, the introduction of Sn^{4+} affects the three phase transition temperatures. As shown in fig. 5b, c) a down shift of the T_{T-C} transition temperature is observed when increasing of Sn-content. Whereas a reverse trend is observed for the T_{R-O} and T_{O-T} phase transition temperatures where a significant upshift is occurring with the increasing Sn-content as reported elsewhere [1,28].

Recall that in the R-phase of BT, the polarization aligns parallel to the (111) axis, whereas it is parallel to the (011) axis in the O-phase, (001) axis in the T-phase, and vanishes in the C-phase [55]. The Sn incorporation in the BT matrix, impedes the Ti-polar displacement leading to a disturbance of the long-range Coulomb potential. Laulhé *et al.* [56], by using first principles supercell calculation on $BaTi_{0.75}Zr_{0.26}O_3$ (a homovalent substitution as in our case), reported that the type of a Ti-displacement is determined by the Ti/Zr distribution in the adjacent local strain effects, which is governed by the size difference between Ti and Zr atoms. Furthermore, Keeble *et al.* [57] on studying BCZT system, reported that the reduction of the number of Ti^{4+} $(111)_{pc}$ displacements is originated from a competition between A-site and B-site polar instabilities.

Indeed, we surmise that the involvement of two different octahedral environments in the system (Ti-O and Sn-O), disturb the off-centering displacement of Ti ions in BTxSn system leading to the observed shifts of the phase transition temperatures.

Besides, from figure 5, we can observe a broadening of the sharp T_C transition temperature in the presence of Sn^{4+} ions, revealing the evolving disorder in the BTxSn system. These results are in good agreement with our vibrational investigations, showing a reduction of the long-range FE ordering along with an increasing disorder in the system while increasing the Sn content.

In addition, the maximal value of the dielectric permittivity at T_C is observed to dramatically increase up to ~ 18000 for BT7.5%Sn system. Hence, we surmise that the presence of Sn is responsible for the increased dielectric constant owing to the induced PNRs in the BTxSn system, as reported by Shi *et al.* using high-resolution transmission electron microscopy [27]. Furthermore, high dielectric constants are commonly reported for relaxor ferroelectrics to be associated to the presence of PNRs [58]. Besides, the increased grain size in the case of the doped

materials (2-3 µm for BTxSn instead of 70 nm for BT) could also be responsible for this enhancement.

3.5. Ferroelectric properties and stored energy

To examine the ferroelectric properties of processed samples, P-E loops were recorded as a function of temperature. Fig. 6 depicts the hysteresis loops of the three samples captured around their Curie temperatures.

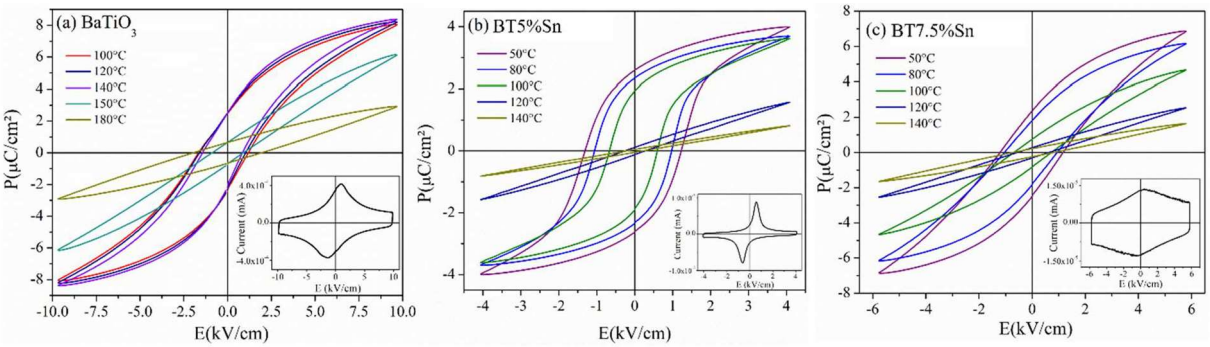

Fig. 6. Temperature dependence of the ferroelectric hysteresis loops: $BaTiO_3$, b) $BaTi_{0.95}Sn_{0.05}O_3$, and c) $BaTi_{0.925}Sn_{0.075}O_3$. The insets show their corresponding polarization current curves at 100°C.

The neat BT compound (e.g., fig. 6a), exhibits narrow hysteresis loops with a corresponding maximum polarization of P_{max} = 8µC/cm^2, low remanent polarization P_r = 2µC/cm^2 and low coercive field E_c = 1kV/cm, in the FE phase. These narrow hysteresis loops compared to the saturated loops usually obtained in the bulk system are mainly due to the grain size effects as commonly admitted [59]. In contrast, the P-E loops appear to have square-like shape signature of saturated P-E hysteresis loops for the BT5%Sn (e.g., fig. 6b) indicating a reinforced FE activity at this Sn concentration visible by the sharp current peak obtained (e.g., inset of fig. 6b). This agrees with reported study carried out on BTxSn compounds having higher grain size (50 – 70 µm) [26], which seems to remain valid for our BTxSn doped compound. However, a different trend is observed for BT doped with 7.5%Sn content (e.g., fig. 6c), although the P-E loops are wider than the ones obtained for neat BT, they remain narrow in comparison with the BT5%Sn. This is coherent with the broader integrated current peaks observed for BT7.5%Sn, which is the signature of the presence of disorder or to several polarized nano-regions.

Moreover, the significant decrease of the coercive field from 1.4 kV/cm for neat BT to 0.6 kV/cm for BT5%Sn, reveals an easier polarization switching of the FE domains.

To examine the grain size effects on the energy storage performances of the nanostructured BTxSn, we have computed the recoverable energy density (W_{rec}) and energy efficiency (η) as described elsewhere [60]. The obtained results are reported in fig. 7.

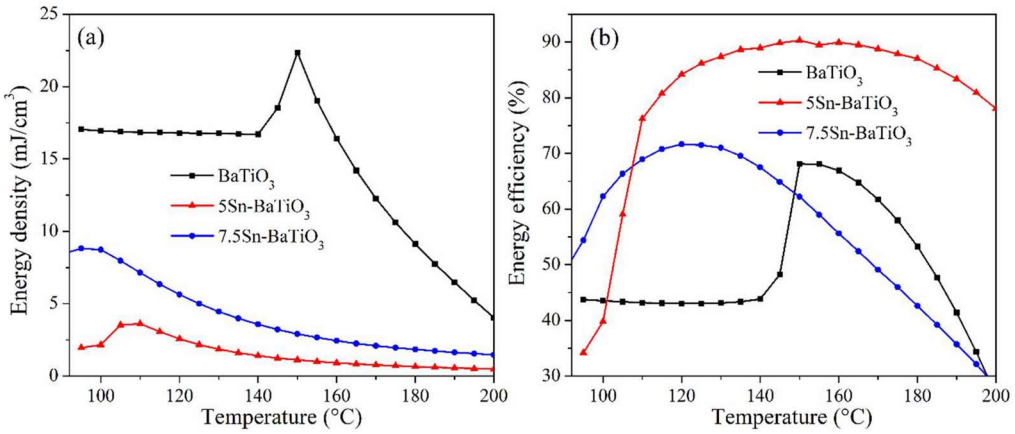

Fig. 7. a) Energy storage density and b) energy efficiency of $BaTi_{1-x}Sn_xO_3$.

Regarding the neat BT system, high yield stability was observed in the temperature range 95-140°C with W_{rec} = 17.4 mJ/cm^3 and η = 43% and a maximum of 23 mJ/cm^3 with a high energy efficiency of 67%. Remind that in neat BT, significant energy storage performances are not expected due to the quasi-square hysteresis loop observed in the bulk system and relatively low surface of stored energy in P-E loops. In the PE region, a drastic decrease of the recoverable energy is observed in the BT5%Sn and BT7.5%Sn compared to the neat BT. However higher energy efficiency ~ 90% was obtained for BT5%Sn, in a large range of temperatures. Thus, Sn^{4+} ions appear to be an adjusting parameter to control the energy storage performances in BTxSn system. Therefore, the BT5%Sn has a great potential to be considered as low energy consumption in nano-cooling devices.

3.6. Electrocaloric effect investigations

It is worth noting that various experimental techniques were developed to directly measure and extract the EC effect such as differential scanning calorimetry [61], the modified high-resolution calorimetry [62], the fast infrared photometry [63], and the scanning thermal microscopy [64]. Besides, since the EC effect is a thermodynamic phenomenon, it can be indirectly evaluated using Maxwell equations as reported elsewhere [61]. Using the indirect approach, in this work, P-E hysteresis loops data were used to extract the EC adiabatic temperature change in BTxSn as a function of temperature. This indirect determination of EC effect, based on Maxwell equations, is

described elsewhere [61]. Note that the cyclic application of an electric field on a FE material leads to an entropy change, which is at the origin of temperature variations in the system giving rise to the EC effect, where the adiabatic temperature change is estimated using the following equation:

$$\Delta T = -\frac{1}{\rho C_p}\int_{E_1}^{E_2} T\left(\frac{\partial P}{\partial T}\right) dE \qquad 1$$

where $E_{1,2}$ stands for the initial and final applied electric fields, P represents the polarization. ρ and C_p correspond to the density of the neat BT, BT5%Sn and BT7.5%Sn respectively, 6.034, 6.090, 6.129 g/cm^3 and to thermal heat capacity 550, 450, 430 J/K Kg. Fig. 8 gives the temperature dependent of EC temperature change of BTxSn samples with respect to the applied electric fields.

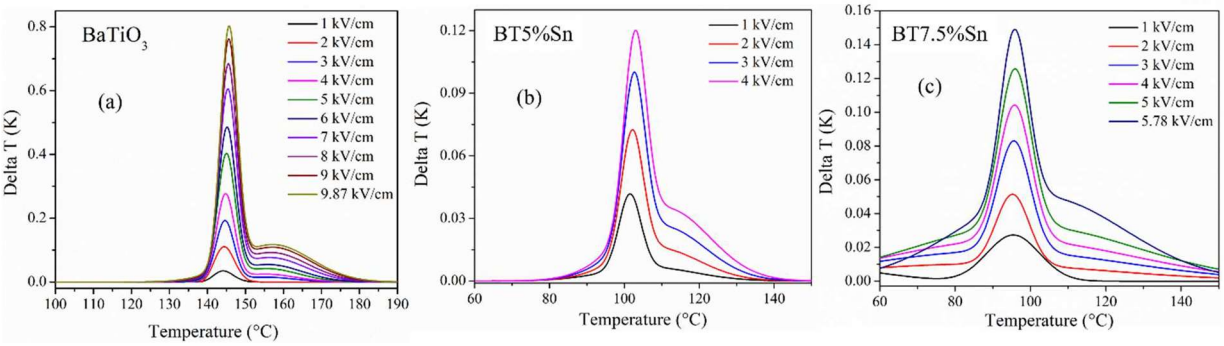

Fig. 8. Temperature and electric field dependence of the adiabatic temperature change (ΔT) of a) $BaTiO_3$, b) $BaTi_{0.95}Sn_{0.05}O_3$, and c) $BaTi_{0.925}Sn_{0.075}O_3$ systems.

These EC temperature change curves show the FE-to-PE phase transitions in the BTxSn samples where maximal ΔT is obtained at T_C. It is worth to note the presence of an evident enlargement of the EC peak at T_C with increasing Sn-content, which corroborates with the existence of polarized nano-regions in doped BT induced by the incorporation of Sn. Furthermore, a slight peak shoulder seems to appear at specific applied electric fields, and it is more pronounced at high electric fields at around 160°C, 120°C, and 110°C for neat BT, BT 5%Sn, and BT 7.5%Sn, respectively.

This peak might be attributed to the hard switching dynamics of the PNRs, which are assumed to be hard to undergo changes of their orientations at T_C and needed higher temperatures and applied electric fields to achieve the switching. The increasing of Sn-content induced the shift of the shoulder position towards the main EC peak, which could lead to the merge of both peaks at

higher Sn-content. This will result in one broad EC peak presenting high temperature stability suitable for cooling devices.

Table 3 summarizes the obtained EC performances of the BTxSn samples at T_C, compared to some other BT-based systems [26,65–67].

Table 3. Electrocaloric performances obtained in this work compared to other literature data of BT-based systems.

Composition	ΔT (K) at T_C	ΔE (kV/cm)	ΔT/ ΔE × 10^{-6} (K.m/V)	Grain size (μm)	Synthesis method
$BaTiO_3$ This work	0.80	9.87	0.81	~ 0.07	Modified Pechini
$BaTi_{0.95}Sn_{0.05}O_3$ This work	0.12	4.07	0.29	~ 2	Modified Pechini
$BaTi_{0.925}Sn_{0.075}O_3$ This work	0.15	5.78	0.26	~ 3	Modified Pechini
$BaTiO_3$ [26]	0.01	9.98	0.1	~0.5	Solid-state reaction
$BaTi_{0.95}Sn_{0.05}O_3$ [26]	0.079	3.62	0.21	~50	Solid-state reaction
$BaTi_{0.9}Sn_{0.1}O_3$ [26]	0.05	10.13	0.049	~25	Solid-state reaction
$Ba_{0.8}Ca_{0.2}TiO_3$[65]	0.12	7.95	0.15	~8	Solid-state reaction
$Ba_{0.975}La_{0.017}(Zr_{0.05}Ti_{0.90})Sn_{0.05}O_3$[66]	0.243	12	0.20	~0.4	Solid-state reaction
$Ba_{0.85}Ca_{0.15}Ti_{0.90}Zr_{0.1}O_3$[67]	0.109	6.65	0.16	-	Solvothermal

As can be observed, a high value of the adiabatic temperature change is obtained for the nanostructured neat BT system, namely ΔT = 0.8 K at 9.87 kV/cm, with a significant corresponding responsivity of $\Delta T/\Delta E = 0.81\times10^{-6}$ K m/V. In comparison to bulk BT elaborated via solid-state method, a clear weak responsivity of 0.1×10^{-6} K m/V was reported [26]. Thus, the EC effect appears to be maximized in nanostructured neat BT used in this study, which was processed via modified Pechini method; especially higher responsivity is obtained to be compared to the one of BT system with micrometric grain size. These results are comparable to the work reported by Moya *et al.* [68] where an important EC responsivity of $\Delta T/\Delta E = 0.75\times10^{-6}$ K m/V, was obtained in commercial single-crystal $BaTiO_3$ sample. In contrast, low EC responses were reported for commercial multilayer ceramic capacitors (MLCC) based on BT system (Y5V capacitor type) of $\Delta T/\Delta E < 0.06\times10^{-6}$ K m/V [64,69].

Moreover, in this work, the Sn doped BT ceramics prepared using the modified Pechini method present an improved EC responsivity compared to similar compositions synthesized using the conventional solid-state method (see Table 3). In particular, BT5%Sn, and BT7.5%Sn samples exhibited an important EC responsivity, respectively of 0.29×10^{-6}, and 0.26×10^{-6} K m/V at T_C.

4. Conclusions

Nanostructured lead-free $BaTi_{1-x}Sn_xO_3$ (x = 0, 0.05 and 0.075) were successfully elaborated using modified Pechini method. For neat $BaTiO_3$, phase symmetry is confirmed to match with tetragonal symmetry (*P*4*mm,* No 99) while orthorhombic symmetry phase (*A*2*mm,* No 38) was confirmed for doped $BaTiO_3$ with 5%Sn and 7.5%Sn contents. Dielectric properties investigations confirmed phase transition temperatures in this system and the enhancement of the dielectric permittivity with increasing Sn-content. The Curie temperature up shifted towards higher temperatures was observed in neat BT T_C = 139°C, compared to 120°C reported for BT bulk material. Therefore, the incorporation of a small amount of Sn in the BT host lattice was found to lower T_C. Electrocaloric effects and energy storage properties were examined for the investigated samples. Remarkably, a high electrocaloric responsivity was obtained for the nanostructured neat BT, which greatly exceeds the reported values for the equivalent bulk materials that deserves vivid interest for developing new refrigeration devices based on nanostructured BT compound.

Acknowledgements

This research was funded by a seed grant provided by "Alliance A2U". Authors are grateful to the University of Picardie Jules Verne Electron Microscopy facility.

References:

[1] L. Xie, Y.L. Li, R. Yu, Z.Y. Cheng, X.Y. Wei, X. Yao, C.L. Jia, K. Urban, A.A. Bokov, Z.-G. Ye, J. Zhu, Static and dynamic polar nanoregions in relaxor ferroelectric BaTi1-xSnxO3 system at high temperature, Physical Review B. 85 (2012) 14118. https://doi.org/10.1103/PhysRevB.85.014118.

[2] X. Yang, Y. Liu, C. He, H. Tailor, X. Long, La-modified Pb(Lu1/2Nb1/2)O3 antiferroelectric ceramics with high energy storage density, Journal of the European Ceramic Society. 35 (2015) 4173–4180. https://doi.org/https://doi.org/10.1016/j.jeurceramsoc.2015.07.027.

[3] A.S. Mischenko, Q. Zhang, R.W. Whatmore, J.F. Scott, N.D. Mathur, Giant electrocaloric effect in the thin film relaxor ferroelectric 0.9PbMg1⁄3Nb2⁄3O3–0.1PbTiO3 near room temperature, Applied Physics Letters. 89 (2006) 242912. https://doi.org/10.1063/1.2405889.

[4] EUR-Lex - 32011L0065 - EN - EUR-Lex, (n.d.). https://eur-lex.europa.eu/legal-content/en/TXT/?uri=CELEX:32011L0065 (accessed September 9, 2021).

[5] Z. Sun, Z. Wang, Y. Tian, G. Wang, W. Wang, M. Yang, X. Wang, F. Zhang, Y. Pu, Progress, Outlook, and Challenges in Lead-Free Energy-Storage Ferroelectrics, Advanced Electronic Materials. 6 (2020) 1900698. https://doi.org/https://doi.org/10.1002/aelm.201900698.

[6] T.R. Shrout, S.J. Zhang, Lead-free piezoelectric ceramics: Alternatives for PZT?, Journal of Electroceramics. 19 (2007) 113–126.

[7] S.O. Leontsev, R.E. Eitel, Progress in engineering high strain lead-free piezoelectric ceramics, Science and Technology of Advanced Materials. 11 (2010) 44302. https://doi.org/10.1088/1468-6996/11/4/044302.

[8] M. Maraj, W. Wei, B. Peng, W. Sun, Dielectric and Energy Storage Properties of Ba(1−x)CaxZryTi(1−y)O3 (BCZT): A Review, Materials . 12 (2019). https://doi.org/10.3390/ma12213641.

[9] M.T. Buscaglia, M. Viviani, V. Buscaglia, L. Mitoseriu, A. Testino, P. Nanni, Z. Zhao, M. Nygren, C. Harnagea, D. Piazza, C. Galassi, High dielectric constant and frozen macroscopic polarization in dense nanocrystalline BaTiO3 ceramics, Physical Review B. 73 (2006) 64114. https://doi.org/10.1103/PhysRevB.73.064114.

[10] V. Buscaglia, M.T. Buscaglia, M. Viviani, T. Ostapchuk, I. Gregora, J. Petzelt, L. Mitoseriu, P. Nanni, A. Testino, R. Calderone, C. Harnagea, Z. Zhao, M. Nygren, Raman and AFM piezoresponse study of dense BaTiO3 nanocrystalline ceramics, Journal of the European Ceramic Society. 25 (2005) 3059–3062. https://doi.org/https://doi.org/10.1016/j.jeurceramsoc.2005.03.190.

[11] S. Tusseau-Nenez, J.-P. Ganne, M. Maglione, A. Morell, J.-C. Niepce, M. Paté, BST ceramics: Effect of attrition milling on dielectric properties, Journal of the European Ceramic Society. 24 (2004) 3003–3011. https://doi.org/https://doi.org/10.1016/j.jeurceramsoc.2003.11.019.

[12] L. Veselinović, M. Mitrić, L. Mančić, M. Vukomanović, B. Hadžić, S. Marković, D. Uskoković, The effect of Sn for Ti substitution on the average and local crystal structure of BaTi1-xSnxO3 (0«x«0.20), Journal of Applied Crystallography. 47 (2014) 999–1007. https://doi.org/10.1107/S1600576714007584.

[13] H. Ghayour, M. Abdellahi, A brief review of the effect of grain size variation on the electrical properties of BaTiO3-based ceramics, Powder Technology. 292 (2016) 84–93. https://doi.org/https://doi.org/10.1016/j.powtec.2016.01.030.

[14] Y.(白洋) Bai, X.(韩茜) Han, K.(丁凯) Ding, L.-J.(乔利杰) Qiao, Combined effects of diffuse phase transition and microstructure on the electrocaloric effect in Ba1−xSrxTiO3 ceramics, Applied Physics Letters. 103 (2013) 162902. https://doi.org/10.1063/1.4825266.

[15] S. Kar-Narayan, N.D. Mathur, Direct and indirect electrocaloric measurements using multilayer capacitors, Journal of Physics D: Applied Physics. 43 (2010) 32002. https://doi.org/10.1088/0022-3727/43/3/032002.

[16] X. Moya, E. Stern-Taulats, S. Crossley, D. González-Alonso, S. Kar-Narayan, A. Planes, L. Mañosa, N.D. Mathur, Giant Electrocaloric Strength in Single-Crystal BaTiO3, Advanced Materials. 25 (2013) 1360–1365. https://doi.org/https://doi.org/10.1002/adma.201203823.

[17] A.R. West, Basic solid state chemistry, John Wiley \& Sons Incorporated, 1999.

[18] D.L. Shan, C.H. Lei, Y.C. Cai, K. Pan, Y.Y. Liu, Mechanical control of electrocaloric response in epitaxial ferroelectric thin films, International Journal of Solids and Structures. 216 (2021) 59–67. https://doi.org/https://doi.org/10.1016/j.ijsolstr.2021.01.020.

[19] D. Shan, Y. Cai, C. Lei, J. Peng, N. He, K. Pan, Y. Liu, J. Li, Electric-field-driven coexistence of positive and negative electrocaloric effects near room temperature for high-efficiency two-stage cooling, Applied Physics Letters. 118 (2021) 122905. https://doi.org/10.1063/5.0047020.

[20] S. Liu, Q. Xie, L. Zhang, Y. Zhao, X. Wang, P. Mao, J. Wang, X. Lou, Tunable electrocaloric and energy storage behavior in the Ce, Mn hybrid doped BaTiO3 ceramics, Journal of the European Ceramic Society. 38 (2018) 4664–4669. https://doi.org/https://doi.org/10.1016/j.jeurceramsoc.2018.06.020.

[21] X. Wang, F. Tian, C. Zhao, J. Wu, Y. Liu, B. Dkhil, M. Zhang, Z. Gao, X. Lou, Giant electrocaloric effect in lead-free Ba0.94Ca0.06Ti1−xSnxO3 ceramics with tunable Curie temperature, Applied Physics Letters. 107 (2015) 252905. https://doi.org/10.1063/1.4938134.

[22] G. Singh, V.S. Tiwari, P.K. Gupta, Electro-caloric effect in (Ba1−xCax)(Zr0.05Ti0.95)O3: A lead-free ferroelectric material, Applied Physics Letters. 103 (2013) 202903. https://doi.org/10.1063/1.4829635.

[23] Z. Luo, D. Zhang, Y. Liu, D. Zhou, Y. Yao, C. Liu, B. Dkhil, X. Ren, X. Lou, Enhanced electrocaloric effect in lead-free BaTi1−xSnxO3 ceramics near room temperature, Applied Physics Letters. 105 (2014) 102904. https://doi.org/10.1063/1.4895615.

[24] Y. Zhang, Thermal hysteresis and electrocaloric effect in Ba1-xZrxTiO3, Journal of Physics and Chemistry of Solids. 115 (2018) 326–331. https://doi.org/https://doi.org/10.1016/j.jpcs.2017.12.043.

[25] J. Li, D. Zhang, S. Qin, T. Li, M. Wu, D. Wang, Y. Bai, X. Lou, Large room-temperature electrocaloric effect in lead-free BaHfxTi1−xO3 ceramics under low electric field, Acta Materialia. 115 (2016) 58–67. https://doi.org/https://doi.org/10.1016/j.actamat.2016.05.044.

[26] S.K. Upadhyay, V.R. Reddy, P. Bag, R. Rawat, S.M. Gupta, A. Gupta, Electro-caloric effect in lead-free Sn doped BaTiO3 ceramics at room temperature and low applied fields, Applied Physics Letters. 105 (2014) 112907. https://doi.org/10.1063/1.4896044.

[27] T. Shi, L. Xie, L. Gu, J. Zhu, Why Sn doping significantly enhances the dielectric properties of Ba(Ti1-xSnx)O3, Scientific Reports. 5 (2015) 8606. https://doi.org/10.1038/srep08606.

[28] C. Lei, A.A. Bokov, Z.-G. Ye, Ferroelectric to relaxor crossover and dielectric phase diagram in the BaTiO3–BaSnO3 system, Journal of Applied Physics. 101 (2007) 84105. https://doi.org/10.1063/1.2715522.

[29] M. Kumar, A. Kumar, Y. Kumar, S. Dhiman, U. Shankar, K.L. Yadav, G. Sharma, Strongly enhanced electrocaloric effects in doped BaTiO3 with reduced grain size, Smart Materials and Structures. 28 (2018) 15013. https://doi.org/10.1088/1361-665x/aae86c.

[30] S. Schlag, H.-F. Eicke, Size driven phase transition in nanocrystalline BaTiO3, Solid State Communications. 91 (1994) 883–887. https://doi.org/https://doi.org/10.1016/0038-1098(94)90007-8.

[31] S. Patel, M. Kumar, Influence of grain size on the electrocaloric and pyroelectric properties in non-reducible BaTiO3 ceramics, AIP Advances. 10 (2020) 85302. https://doi.org/10.1063/5.0017348.

[32] T.O.L. Sunde, T. Grande, M.-A. Einarsrud, Modified pechini synthesis of oxide powders and thin films, Handbook of Sol-Gel Science and Technology. (2016).

[33] W. Li, Z. Xu, R. Chu, P. Fu, J. Hao, Structure and electrical properties of BaTiO3 prepared by sol–gel process, Journal of Alloys and Compounds. 482 (2009) 137–140. https://doi.org/https://doi.org/10.1016/j.jallcom.2009.02.137.

[34] S. Sandin, A. Cheritat, J. Backstrom, A. Cornell, Deposition efficiency in the preparation of ozone-producing nickel and antimony doped tin oxide anodes, Journal of Electrochemical Science and Engineering. 7 (2017) 51–64.

[35] T. Roisnel, J. Rodríquez-Carvajal, WinPLOTR: A Windows Tool for Powder Diffraction Pattern Analysis, Materials Science Forum. 378–381 (2001) 118–123. https://doi.org/10.4028/www.scientific.net/MSF.378-381.118.

[36] R.H. Buttner, E.N. Maslen, Structural parameters and electron difference density in BaTiO3, Acta Crystallographica Section B: Structural Science. 48 (1992) 764–769.

[37] A.R. Denton, N.W. Ashcroft, Vegard's law, Phys. Rev. A. 43 (1991) 3161–3164. https://doi.org/10.1103/PhysRevA.43.3161.

[38] S. Saitzek, J.-F. Blach, S. Villain, J.-R. Gavarri, Nanostructured ceria: a comparative study from X-ray diffraction, Raman spectroscopy and BET specific surface measurements, Physica Status Solidi (a). 205 (2008) 1534–1539. https://doi.org/https://doi.org/10.1002/pssa.200723419.

[39] S. Patel, M. Kumar, Influence of grain size on the electrocaloric and pyroelectric properties in non-reducible BaTiO3 ceramics, AIP Advances. 10 (2020) 085302. https://doi.org/10.1063/5.0017348.

[40] M. Kumar, A. Kumar, Y. Kumar, S. Dhiman, U. Shankar, K.L. Yadav, G. Sharma, Strongly enhanced electrocaloric effects in doped BaTiO3 with reduced grain size, Smart Materials and Structures. 28 (2018) 15013.

[41] R. Selvamani, G. Singh, V. Sathe, V.S. Tiwari, P.K. Gupta, Dielectric, structural and Raman studies on (Na0.5Bi0.5TiO3)(1 −x)(BiCrO3)xceramic, Journal of Physics: Condensed Matter. 23 (2011) 55901. https://doi.org/10.1088/0953-8984/23/5/055901.

[42] F. Lawar, J. Belhadi, B. Asbani, B. Manoun, H. Kaddoussi, M. Courty, C. Boudaya, M. El Marssi, H. Khemakhem, A. Lahmar, Structural investigation, dielectric, ferroelectric, and elecrocaloric properties of lead-free Ba(1−x)CaxTi(1−x)(Li1/3Nb2/3)xO3−δ (x = 0.02 and x = 0.07) ceramics, Journal of Materials Science: Materials in Electronics. 29 (2018) 18640–18649. https://doi.org/10.1007/s10854-018-9983-2.

[43] G. Schileo, L. Luisman, A. Feteira, M. Deluca, K. Reichmann, Structure–property relationships in BaTiO3–BiFeO3–BiYbO3 ceramics, Journal of the European Ceramic Society. 33 (2013) 1457–1468. https://doi.org/https://doi.org/10.1016/j.jeurceramsoc.2013.01.011.

[44] K. Laabidi, M.D. Fontana, B. Jannot, Underdamped soft phonon in orthorhombic BaTiO3, Solid State Communications. 76 (1990) 765–768. https://doi.org/https://doi.org/10.1016/0038-1098(90)90623-J.

[45] P.S. Dobal, A. Dixit, R.S. Katiyar, D. Garcia, R. Guo, A.S. Bhalla, Micro-Raman study of Ba1 − xSrxTiO3 ceramics, Journal of Raman Spectroscopy. 32 (2001) 147–149. https://doi.org/https://doi.org/10.1002/jrs.681.

[46] U.D. Venkateswaran, V.M. Naik, R. Naik, High-pressure Raman studies of polycrystalline ${\mathrm{BaTiO}}_{3}$, Phys. Rev. B. 58 (1998) 14256–14260. https://doi.org/10.1103/PhysRevB.58.14256.

[47] J. JAVADPOUR, N.G. EROR, Raman Spectroscopy of Higher Titanate Phases in the BaTiO3-TiO2 System, Journal of the American Ceramic Society. 71 (1988) 206–213. https://doi.org/https://doi.org/10.1111/j.1151-2916.1988.tb05849.x.

[48] N. Baskaran, A. Ghule, C. Bhongale, R. Murugan, H. Chang, Phase transformation studies of ceramic BaTiO3 using thermo-Raman and dielectric constant measurements, Journal of Applied Physics. 91 (2002) 10038–10043. https://doi.org/10.1063/1.1481771.

[49] O.A. Maslova, Y.I. Yuzyuk, M. Jain, S.A. Barannikova, Lattice Dynamics of Barium Titanate: Single Crystal, Ceramic, and Polycrystalline Film, Physica Status Solidi (b). 257 (2020) 1900762. https://doi.org/https://doi.org/10.1002/pssb.201900762.

[50] D.-Y. Lu, X.-Y. Sun, M. Toda, A novel high-k 'Y5V' barium titanate ceramics co-doped with lanthanum and cerium, Journal of Physics and Chemistry of Solids. 68 (2007) 650–664. https://doi.org/https://doi.org/10.1016/j.jpcs.2007.02.018.

[51] R. Farhi, M. El Marssi, A. Simon, J. Ravez, A Raman and dielectric study of ferroelectric ceramics, The European Physical Journal B - Condensed Matter and Complex Systems. 9 (1999) 599–604. https://doi.org/10.1007/s100510050803.

[52] S.K. Upadhyay, V.R. Reddy, K. Sharma, A. Gome, A. Gupta, Study of Aging & De-Aging Behaviour in Un-Doped Polycrystalline Ferroelectric BaTiO3, Ferroelectrics. 437 (2012) 171–180. https://doi.org/10.1080/00150193.2012.738590.

[53] H. Tian, B. Yao, C. Hu, X. Meng, Z. Zhou, Impact of polar nanoregions on the quadratic electro-optic effect in K0.95Na0.05Ta1−xNbxO3crystals near the Curie temperature, Applied Physics Express. 7 (2014) 62601. https://doi.org/10.7567/apex.7.062601.

[54] C. Fang, L. Chen, D. Zhou, Influence of domain on grain size effects of the dielectric properties of BaTiO3 nanoceramics and nanoparticles, Physica B: Condensed Matter. 409 (2013) 83–86. https://doi.org/https://doi.org/10.1016/j.physb.2012.10.016.

[55] B. Ravel, E.A. Stern, R.I. Vedrinskii, V. Kraizman, Local structure and the phase transitions of BaTiO3, Ferroelectrics. 206 (1998) 407–430.

[56] C. Laulhé, A. Pasturel, F. Hippert, J. Kreisel, Random local strain effects in homovalent-substituted relaxor ferroelectrics: A first-principles study of ${\text{BaTi}}_{0.74}{\text{Zr}}_{0.26}{\text{O}}_{3}$, Physical Review B. 82 (2010) 132102. https://doi.org/10.1103/PhysRevB.82.132102.

[57] D.S. Keeble, F. Benabdallah, P.A. Thomas, M. Maglione, J. Kreisel, Revised structural phase diagram of (Ba0.7Ca0.3TiO3)-(BaZr0.2Ti0.8O3), Applied Physics Letters. 102 (2013) 092903. https://doi.org/10.1063/1.4793400.

[58] L.E. Cross, Relaxor ferroelectrics, Ferroelectrics. 76 (1987) 241–267. https://doi.org/10.1080/00150198708016945.

[59] F.Q. Guo, B.H. Zhang, Z.X. Fan, X. Peng, Q. Yang, Y.X. Dong, R.R. Chen, Grain size effects on piezoelectric properties of BaTiO 3 ceramics prepared by spark plasma sintering, Journal of Materials Science: Materials in Electronics. 27 (2016) 5967–5971.

[60] M. Benyoussef, M. Zannen, J. Belhadi, B. Manoun, Z. Kutnjak, D. Vengust, M. Spreitzer, M. El Marssi, A. Lahmar, Structural, dielectric, and ferroelectric properties of Na0.5(Bi1-xNdx)0.5TiO3 ceramics for energy storage and electrocaloric applications, Ceramics International. 47 (2021) 26539–26551. https://doi.org/https://doi.org/10.1016/j.ceramint.2021.06.068.

[61] Z. Kutnjak, B. Rožič, R. Pirc, Electrocaloric Effect: Theory, Measurements, and Applications, Wiley Encyclopedia of Electrical and Electronics Engineering. (2015) 1–19. https://doi.org/https://doi.org/10.1002/047134608X.W8244.

[62] S. Kumar, J. Brock, Liquid crystals: experimental study of physical properties and phase transitions, Cambridge University Press, 2001.

[63] B. Rožič, M. Kosec, H. Uršič, J. Holc, B. Malič, Q.M. Zhang, R. Blinc, R. Pirc, Z. Kutnjak, Influence of the critical point on the electrocaloric response of relaxor ferroelectrics, Journal of Applied Physics. 110 (2011) 064118. https://doi.org/10.1063/1.3641975.

[64] D. Shan, K. Pan, Y. Liu, J. Li, High fidelity direct measurement of local electrocaloric effect by scanning thermal microscopy, Nano Energy. 67 (2020) 104203. https://doi.org/https://doi.org/10.1016/j.nanoen.2019.104203.

[65] B. Asbani, J.-L. Dellis, A. Lahmar, M. Courty, M. Amjoud, Y. Gagou, K. Djellab, D. Mezzane, Z. Kutnjak, M. El Marssi, Lead-free Ba0.8Ca0.2(ZrxTi1−x)O3 ceramics with large electrocaloric effect, Applied Physics Letters. 106 (2015) 42902. https://doi.org/10.1063/1.4906864.

[66] S. Smail, M. Benyoussef, K. Taïbi, N. Bensemma, B. Manoun, M. El Marssi, A. Lahmar, Structural, dielectric, electrocaloric and energy storage properties of lead free Ba0.975La0.017(ZrxTi0.95-x)Sn0.05O3 (x = 0.05; 0.20) ceramics, Materials Chemistry and Physics. 252 (2020) 123462. https://doi.org/https://doi.org/10.1016/j.matchemphys.2020.123462.

[67] Z. Hanani, D. Mezzane, M. Amjoud, A.G. Razumnaya, S. Fourcade, Y. Gagou, K. Hoummada, M. El Marssi, M. Gouné, Phase transitions, energy storage performances and electrocaloric effect of the lead-free Ba0.85Ca0.15Zr0.10Ti0.90O3 ceramic relaxor, Journal of Materials Science: Materials in Electronics. 30 (2019) 6430–6438. https://doi.org/10.1007/s10854-019-00946-5.

[68] X. Moya, E. Stern-Taulats, S. Crossley, D. González-Alonso, S. Kar-Narayan, A. Planes, L. Mañosa, N.D. Mathur, Giant Electrocaloric Strength in Single-Crystal BaTiO3, Advanced Materials. 25 (2013) 1360–1365. https://doi.org/https://doi.org/10.1002/adma.201203823.

[69] B. Lu, X. Wen, Z. Tang, B. Liang, T. Tao, Z. Xie, T. Zhang, X. Tang, Y. Xiang, J. Liao, S. Lu, Large electrocaloric effect in BaTiO3 based multilayer ceramic capacitors, Science China Technological Sciences. 59 (2016) 1054–1058. https://doi.org/10.1007/s11431-016-6079-1.